Physics and Astronomy Faculty Publications

Physics and Astronomy

1-2012

Photocatalytic Hydrogen Production at Titania-Supported Pt Nanoclusters that are Derived from Surface-Anchored Molecular Precursors

Rony S. Khnayzer

Lucas B. Thompson

Mikhail Zamkov
Bowling Green State University, zamkovm@bgsu.edu

Shane Ardo

Gerald J. Meyer

See next page for additional authors

Repository Citation

Author(s)

Rony S. Khnayzer, Lucas B. Thompson, Mikhail Zamkov, Shane Ardo, Gerald J. Meyer, Catherine J. Murphy, and Felix N. Castellano

Photocatalytic Hydrogen Production at Titania-Supported Pt Nanoclusters That Are Derived from Surface-Anchored Molecular Precursors

Rony S. Khnayzer,[†,§] Lucas B. Thompson,[‖] Mikhail Zamkov,[‡,§] Shane Ardo,[⊥] Gerald J. Meyer,[⊥] Catherine J. Murphy,[‖] and Felix N. Castellano*[†,§]

[†]Department of Chemistry, [‡]Department of Physics, [§]Center for Photochemical Sciences, Bowling Green State University, Bowling Green, Ohio 43403, United States

[‖]Department of Chemistry, University of Illinois at Urbana–Champaign, Urbana, Illinois 61801, United States

[⊥]Department of Chemistry, Johns Hopkins University, 3400 North Charles Street, Baltimore, Maryland 21218, United States

S Supporting Information

ABSTRACT: Degussa P-25 TiO_2 bearing surface-anchored $Pt(dcbpy)Cl_2$ [dcbpy = 4,4′-dicarboxylic acid-2,2′-bipyridine] prepared with systematically varied surface coverage produced Pt^0 nanoparticles under bandgap illumination in the presence of methanol hole scavengers. Energy-dispersive X-ray spectroscopy confirmed the presence of elemental platinum in the newly formed nanoparticles during scanning transmission electron microscopy (STEM) experiments. According to the statistical analysis of numerous STEM images, the Pt^0 nanoclusters were distributed in a segregated manner throughout the titania surface, ranging in size from 1 to 3 nm in diameter. The final achieved nanoparticle size and net hydrogen production were determined as a function of the $Pt(dcbpy)Cl_2$ surface coverage as well as other systematically varied experimental parameters. The hybrid Pt/TiO_2 nanomaterials obtained upon complete decomposition of the $Pt(dcbpy)Cl_2$ precursor displayed higher photocatalytic activity (300 μmol/h) for hydrogen evolution in aqueous suspensions when compared with platinized TiO_2 derived from H_2PtCl_6 precursors (130 μmol/h), as ascertained through gas chromatographic analysis of the photoreactor headspace under identical experimental conditions. The conclusion that H_2 was evolved from Pt^0 sites rather than from molecular $Pt(dcbpy)Cl_2$ entities was independently supported by Hg and CO poisoning experiments. The formation of small Pt nanoparticles (1.5 nm in diameter) prevail at low surface coverage of $Pt(dcbpy)Cl_2$ on TiO_2 (0.5 to 2% by mass) that exhibit enhanced turnover frequencies with respect to all other materials investigated, including those produced from the in situ photochemical reduction of H_2PtCl_6. Pt^{II} precursor absorption in the ultraviolet region appeared to be partially responsible for attenuation of the H_2 evolution rate at higher $Pt(dcbpy)Cl_2$ surface coverage. The nanoparticle size and hydrogen evolution characteristics of the surface-anchored materials generated through photodeposition were directly compared with those derived from chemical reduction using $NaBH_4$. Finally, Degussa P-25 thin films deposited on FTO substrates enabled electrochemically induced (−1.0 V vs Ag/AgCl, pH 7.0, phosphate buffer) electron trapping ($TiO_2(e^-)$) throughout the titania. After removal of the applied bias and the anaerobic introduction of $Pt(dcbpy)Cl_2$, the accumulated electrons reduce this molecular species to Pt^0 nanoparticles on the titania electrode surface, as confirmed by TEM measurements, with the concomitant production of H_2 gas. The combined experiments illustrate that $TiO_2(e^-)$ generated with bandgap excitation or via electrochemical bias affords the reduction of $Pt(dcbpy)Cl_2$ to Pt^0 nanoparticles that in turn are responsible for heterogeneous hydrogen gas evolution.
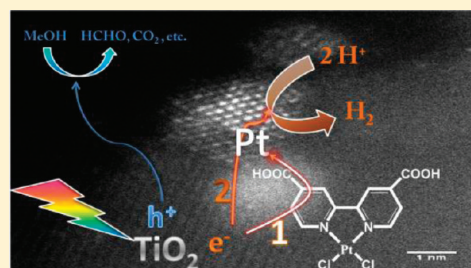
■ INTRODUCTION

The utilization of solar photons for the generation of energy-rich chemical fuels from abundant energy-deficient molecules requires the development of new catalytic systems and redox assemblies.[1−5] Of particular interest is the utilization of sunlight to produce H_2 by the reduction of water, thereby providing an environmentally sensible fuel from naturally abundant precursors.[1−9] The challenge in designing catalysts to promote these reactions lies in the fact that single-photon-driven electron transfer must somehow be coupled to a multielectron fuel-forming step. In other words, the reduction of protons to H_2 requires the coupling

of two protons and two electrons to produce one molecule of the desired combustible fuel. The catalyst serves to bring all reacting species together, permits H_2 evolution, and must ultimately be regenerated to repeat the sequence. Surprisingly, efficient photo-initiated multielectron-transfer chemistry remains largely unrealized in photocatalysis despite decades of research on the subject. The use of metal complexes as molecular photocatalysts for

hydrogen evolution in homogeneous systems has gained wide-spread popularity due to both fundamental mechanistic questions and its possible transformative potential.[10-15] Originally, we were inspired by the notion that molecular catalysts could be readily linked to heterogeneous nanoparticles to yield materials that both absorb light and drive the two-electron reduction of protons to hydrogen gas. During the course of this work, evidence began accumulating that molecular Pt- and Pd-containing complexes were susceptible to photolytic reduction, forming their corresponding metallic nanoparticles, which were ultimately responsible for the majority of H_2 evolution observed in these systems.[16,17] This was not too surprising given the fact that Finke and coworkers previously also noted that the molecular Pt^{II} species $Pt(1,5\text{-COD})Cl_2$ and $Pt(1,5\text{-COD})(CH_3)_2$ (COD is 1,5-cyclooctadiene) both form Pt^0 nanoclusters in situ, the latter being ultimately responsible for substrate hydrogenation catalysis.[18,19] During the course of these studies, we linked $Pt(dcbpy)Cl_2$ (dcbpy is 4,4'-dicarboxy-2,2-bipyridine), originally believed to be a viable molecular hydrogen evolution catalyst,[10-15] to the surface of Degussa P-25 TiO_2, which serve as electron storage reservoirs in the presence of bandgap excitation and appropriate hole scavengers such as methanol.[20] Whereas these composites were indeed superior hydrogen-evolving photocatalysts when directly compared with more conventional materials, they did not function via molecular chemistry at the surface-anchored Pt^{II} complexes.[20] Rather, the Pt^{II} complexes served as molecular precursors that yielded highly segregated nanoscopic Pt^0 particles decorating the TiO_2 surface and formed from bandgap illumination. Notably, this system has been used for aerobic water detoxification under visible-light illumination where the Pt^{II} complex acted as a dye sensitizer that injected electrons into titania initiating a cascade of mineralizing decomposition chemistry of the prototypical 4-chlorophenol.[21]

The work related to nanoparticle-based photodeposition (PD) served as a caveat to researchers employing noble metal-containing complexes as H_2-generating catalysts that photodecomposition of these complexes could in fact occur and that the identity of the true catalysis needs to be rigorously addressed. The present study revealed that surface-bound molecular $Pt(dcbpy)Cl_2$ complexes were photochemical precursors to segregated Pt^0 nanomaterials that displayed enhanced hydrogen evolution from TiO_2 surfaces under bandgap illumination. We view this latter result as significant because the electrocatalytic activity of platinum clusters toward the four-electron reduction of oxygen to water has recently been demonstrated to exhibit drastic size-dependent behavior; smaller nanoparticles (1 to 1.2 nm in diameter) promote enhanced catalytic activity.[22] Variation in Pt^0 particle size may indeed be the reason for the wide variation of H_2 evolution rates we observed as a function of $Pt(dcbpy)Cl_2$ surface coverage on TiO_2 in the original study,[20] and the current effort develops this concept further through photochemical, chemical, and electrochemical reduction processes to prepare nanoscopic Pt^0 clusters on the surface of titania. We chose these three distinct reduction methods based on previous work by Pichat and coworkers, who extensively studied the nanoscopic deposition of Pt on TiO_2 prepared from a variety of codissolved precursors.[23-25] It should also be noted that the ligands present in the $Pt(dcbpy)Cl_2$ precursor likely help stabilize the resultant Pt^0 nanoparticles distributed on the titania surface. The nature of the titania support renders any surface study of the Pt^0 sites experimentally tedious; therefore, research on the aqueous suspended nanoparticles is underway to better understand the nature of the analogous materials produced on titania.[18,26-29]

We clearly demonstrate from heterogeneous poisoning experiments[30,31] that hydrogen-evolving catalytic activity in these hybrid materials emanates from the nanoparticulate catalysts rather than molecular compounds. The combined data revealed that the H_2 evolution yields monitored as a function of $Pt(dcbpy)Cl_2$ surface coverage could be rationalized in terms of three distinct variables: (1) the mass of Pt^0 deposited, (2) the Pt^0 nanoparticle size, and (3) undecomposed Pt^{II} precursors that competitively absorb ultraviolet photons.[32,33]

■ EXPERIMENTAL SECTION

General. ^{1}H NMR spectra were recorded on a Bruker Avance 300 (300 MHz) or Bruker Avance III 500 (500 MHz) spectrometer. All chemical shifts were referenced to the residual solvent signals, and splitting patterns were designated as s (singlet) or d (doublet). UV—vis absorption spectra were measured on a Cary 50 Bio spectrophotometer. A VWR 75HT sonicator was used to sonicate the colloidal suspensions. Raman spectra were acquired on a Renishaw inVia Raman Microscope using 442 nm He—Cd Laser excitation, and IR spectra were measured using an FT-IR spectrometer (JASCO FT/IR-4100) equipped with an ATR accessory. All electrochemical measurements were performed using a BAS Epsilon electrochemistry workstation using a traditional three electrode arrangement.

Materials. P-25 TiO_2 (ca. 80% anatase, 20% rutile; BET area, ca. 50 m^2 g^{-1}) was obtained from Degussa and used as received. Potassium tetrachloroplatinate, hexacholoroplatinic acid hexahydrate, 4,4'-dimethyl-2,2'-bipyridine, and sodium borohydride ($NaBH_4$) were purchased from Aldrich and used without further purification. Fluorine-doped tin oxide (FTO) conducting glass substrates (TEC 15) were purchased from Hartford Glass. Water was deionized using a Barnstead nanopure system. All reagent grade solvents and reactants were used as received. cis-$Pt(DMSO)_2Cl_2$ was synthesized in 90% yield according to the established literature procedure.[34]

TiO_2 Film Formation. FTO conducting glass substrates were cleaned by sonication using a solution of HCl in isopropanol, a solution of soap in water, then finally acetone. The FTO glass was then dried in an oven. A mixture of 3:1 by volume H_2O/CH_3COOH (glacial acetic acid) was mixed slowly with TiO_2 (Degussa P-25) (12 wt %) and hydroxypropylcellulose (6 wt %). This mixture was sonicated and stirred vigorously overnight. The resultant paste was doctor bladed on FTO glass between three Scotch tape layers resulting in a material with ~20 μm thickness and a TiO_2 electrode area of 1 cm^2. The electrode was sintered at 500 °C for 30 min at a heating rate of 5 °C per min and finally cooled to room temperature.

Synthesis. $Pt(dcbpy)Cl_2$. This complex was synthesized according to a slightly modified literature procedure.[35] 4,4'-Dicarboxy-2,2'-bipyridine (dcbpy) was prepared as described in the literature from 4,4'-dimethyl-2,2'-bipyridine.[36] A suspension of 98 mg dcbpy and 212 mg of cis-$Pt(DMSO)_2Cl_2$ were mixed with 40 mL of methanol and refluxed for 8 h in an oil bath at 80 °C. The yellow solid was filtered, washed with methanol and hot ethanol, and then dried under vacuum (77% yield). Anal. Calcd for $C_{12}H_8Cl_2N_2O_4Pt$: C, 28.25; H, 1.58; N, 5.49; Found: C, 28.53; H, 1.81; N, 5.09. ^{1}H NMR (300 MHz, $(CD_3)_2SO$, δ): 9.72 (d, J = 6 Hz, 2H), 9.04 (s, 2 H), 8.24 (d, J = 5.7 Hz, 2H). ^{1}H NMR (500 MHz, D_2O-NaOD, δ): 8.50 (d, J = 6 Hz, 2H), 8.09 (s, 2H), 7.60 (d, J = 5.8 Hz, 2H). FT-IR (ATR, ν(cm^{-1})): 1730, 1619, 1553, 1440, 1412, 1320, and 1233. Raman spectroscopy

(neat powder, λ_{ex} = 442 nm): ν = 1619, 1590, 1553, 1479, and 1278 cm^{-1}.

Pt(dcbpy)Cl$_2$/TiO$_2$ Compositions.[20,21] Pt(dcbpy)Cl$_2$/TiO$_2$, 1% by mass, was synthesized according to the following procedure: 1 mg of Pt(dcbpy)Cl$_2$ was dissolved in 15 mL of water with 50 μL of 0.1 M KOH in a round-bottomed flask equipped with a stir bar. TiO$_2$ (100 mg, Degussa P-25) was added slowly to the solution, sonicated for 1 min, then stirred for 24 h at room temperature. The mixture was centrifuged (10 min, 10 000 rpm) to separate the solid and liquid phases. Afterward, the solution was filtered through a 0.2 μm filter several times to remove the suspended particles, and the absorption spectrum of the filtrate was analyzed to calculate the amount of Pt(dcbpy)Cl$_2$ (λ = 377 nm, ε = 2770 M^{-1} cm^{-1}) that was adsorbed on the surface of TiO$_2$. The final obtained solid was then dried under vacuum.

To prepare other Pt(dcbpy)Cl$_2$/TiO$_2$ surface coverage, the amount of Pt(dcbpy)Cl$_2$ and 0.1 M KOH added were systematically varied. In routine practice, the minimum amount of base (0.1 M KOH) required to dissolve Pt(dcbpy)Cl$_2$ completely was utilized as excess base facilitates desorption of the surface-anchored species. The following percentages by mass were achieved and further characterized: 0.5, 1, 2, 4.27, and 7.05%. All surface coverage loadings cited in this manuscript are by mass equivalents on TiO$_2$ unless otherwise stated.

Photocatalytic Hydrogen Production. *Pt(dcbpy)Cl$_2$/TiO$_2$ Photodeposition.*[20] Photocatalytic reactions were performed in a 50 mL Pyrex round-bottomed flask equipped with a stir bar. All mixtures were sonicated for 1 min before PD and stirred at the same speed during the measurements. A suspension of 25 mg of the Pt(dcbpy)Cl$_2$/TiO$_2$ catalyst at a specific % loading by mass and 25 mL of methanol/water (1:6 by volume) was degassed using the freeze–pump–thaw technique and maintained under an argon atmosphere in a gastight Schlenk line directly linked to a gas chromatograph (GC, Shimadzu GC-8A, argon carrier gas, 5 Å molecular sieve column (Restek), thermal conductivity detector, 0.5 mL gas sample injection, calibrated against known H$_2$/argon gas mixtures). Under our experimental conditions, the retention time of H$_2$ was 1.5 min, well-separated from N$_2$ and O$_2$. Detection of CO$_2$ from the reaction headspace was accomplished using a different custom-made column for gas separation (Supelco). The excitation light source was the broadband output of a 300 W Xe arc lamp (Oriel). The broadband incident power on the reactor was ~1 W/cm^2. The suspension was subjected to continuous band gap irradiation for 5 h, and hydrogen evolution was analyzed throughout the photolysis. The temperature of the suspension after photocatalysis was consistently ≥50 °C. The solid was then collected by centrifugation (10 min, 10 000 rpm). The TiO$_2$ powder isolated after catalysis had a gray color at 1 and 2% loading and yellowish gray (yellow due to remnant undecomposed Pt(dcbpy)Cl$_2$) at higher % loading. (See the Supporting Information for photographs.) The solid was examined by STEM to measure the Pt nanoparticle size. The remaining molecular Pt^{II} complexes on the surface of TiO$_2$ were quantitatively desorbed by treatment with 0.1 M KOH, and the resultant absorption spectra were used to quantify the amount of undecomposed Pt^{II} precursors and the associated absorbance/transmittance in the UV region. Pt^{II} precursors desorbed from TiO$_2$ appear to speciate in the presence of 0.1 M KOH, a behavior well-established for similar Pt^{II} complexes.[37−41] Explicit details regarding the quantification of desorbed Pt^{II} molecules are presented in the Supporting Information. The following percentages

of Pt(dcbpy)Cl$_2$ decomposed on TiO$_2$ (by mass) after 5 h of photoreaction/catalysis were determined: 0.4% at 0.5% loading; 0.77% at 1% loading, 1.1% at 2% loading, 1.1% at 4.27% loading, and 0.7% at 7.05% loading; see Figure 3b. Complete decomposition of the Pt(dcbpy)Cl$_2$ precursor was observed only in samples with ≤2% loading under prolonged photolysis (>7 h), verified by negligible absorbance of desorbed Pt species in the near-visible region. For the Hg poisoning test, which selectively suppresses the hydrogen evolution from heterogeneous noble metal surfaces, the identical experimental setup was used but with the addition of 3 mL of liquid Hg to the reaction mixture.

Benchmark Platinized TiO$_2$ (Benchmark Photodeposition).[25,42] Benchmark photodeposited Pt/TiO$_2$ materials derived from a traditional non-surface-anchored precursor, H$_2$PtCl$_6$·6H$_2$O, were prepared according to a slightly modified literature procedure. In a 50 mL Pyrex round-bottomed flask, 100 mg of P-25 TiO$_2$ was suspended by sonication in a mixture of methanol/water (1:6 by volume). Hexacholoroplatinic acid hexahydrate (1 mg, H$_2$PtCl$_6$·6H$_2$O) was dissolved in the same solvent mixture, added to the TiO$_2$, and stirred for 15 min in the dark. The combined suspension was degassed using the freeze−pump thaw technique; then, argon gas was introduced above the solution. The mixture was irradiated for 5 h using a 300 W Xe arc lamp (Oriel). The resulting grayish solid was collected by centrifugation washed with water and methanol then dried under vacuum. Resultant solid (12 mg) was used to measure hydrogen evolution and compared with 12 mg Pt(dcbpy)Cl$_2$/TiO$_2$ 1% isolated after complete PD using the same procedure described above, and STEM of the powders was taken. The full decomposition of H$_2$PtCl$_6$ was indicated by the negligible absorption of the supernatant after 5 h of continuous photolysis. Because Pt(dcbpy)Cl$_2$ and H$_2$PtCl$_6$·6H$_2$O have comparable molecular weights, the weight percent of Pt metal is approximately the same in both cases (~0.4 wt % Pt in a 1% by mass sample).

Pt(dcbpy)Cl$_2$/TiO$_2$ Chemical Deposition. We suspended 50 mg of Pt(dcbpy)Cl$_2$/TiO$_2$, 1% by mass, in 25 mL of pure methanol containing a large excess of NaBH$_4$ (2 mg). The chemical reduction of Pt(dcbpy)Cl$_2$ into Pt nanoparticles was vigorous; the resulting grayish solid was collected by centrifugation after 5 h, washed with methanol, and dried under vacuum, and STEM of the powder was taken. We used 12 mg of the resultant solid to measure hydrogen evolution and compared with 12 mg Pt(dcbpy)Cl$_2$/TiO$_2$ 1% isolated after complete PD using the same procedure described above.

CO Poisoning. Because CO is a highly toxic gas, the CO poisoning test was performed in a well-vented fume hood. We degassed 10 mg of 1% by mass Pt(dcbpy)Cl$_2$/TiO$_2$ isolated after 5 h of PD in 10 mL of methanol/water (1:6 by volume) for 30 min with argon bubbling in an airtight vial. Another vial containing the same composition was bubbled with CO for 30 min and maintained under 1 atm of CO. Both vials were stirred at the same spin rate and irradiated with a 300 W Xe arc lamp (Oriel), whose output was sent through bifurcated optical fibers (Oriel) to yield simultaneously 200 mW/cm^2 incident power density on each reactor. The hydrogen was detected from the headspace; samples of gas were taken at different time intervals using a 100 μL gastight syringe (Hamilton) and analyzed using the GC system described above.

Materials Characterization. *Scanning Transmission Electron Microscopy and Transmission Electron Microscopy.* Scanning transmission electron microscopy (STEM) data for the Pt nanoparticles were obtained with a JEOL 2010F operating in darkfield STEM mode at 200 keV. Dried TiO$_2$/Pt samples were

1431

dx.doi.org/10.1021/jp206943s |*J. Phys. Chem. C* 2012, 116, 1429–1438
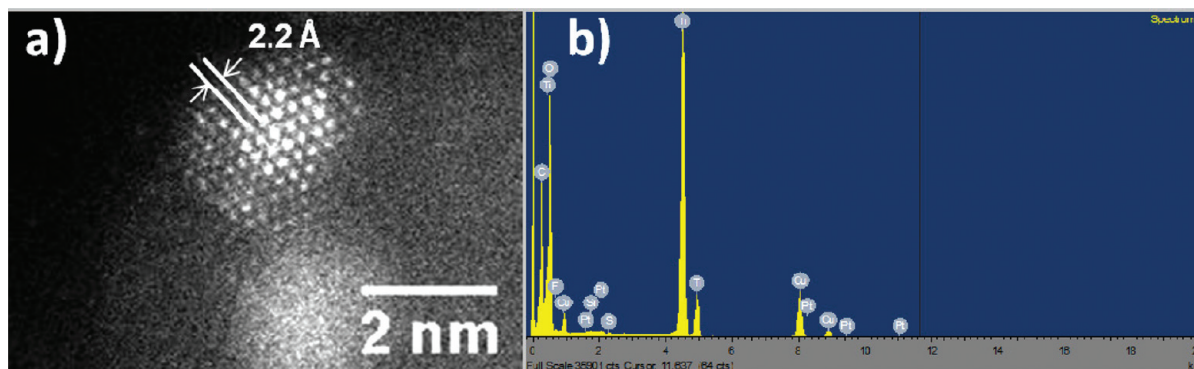
Figure 1. (a) Atomic resolution STEM of 1% Pt(dcbpy)Cl$_2$/TiO$_2$ after 5 h of bandgap illumination, showing nanoscopic platinum particles with high crystallinity indexed to the fcc (111) crystal face, with lattice spacing of 2.2 Å. (b) EDX measurement of the same sample indicating the presence of platinum.

resuspended in ∼200 μL of DI H$_2$O, and ∼20 μL of this solution was dropcasted onto holey carbon transmission electron microscopy (TEM) grids and then dried under ambient laboratory conditions. High-resolution images were acquired with a JEOL model 2200-FS electron microscope operated at 200 keV. EDS scans were acquired with a 50 mm^2 Oxford INCA detector on the 2200FS. High-resolution transmission electron microscopy (HR-TEM) measurements were carried out using a JEOL 3011UHR or 2010 transmission electron microscopes, operated at 300 and 200 kV, respectively.
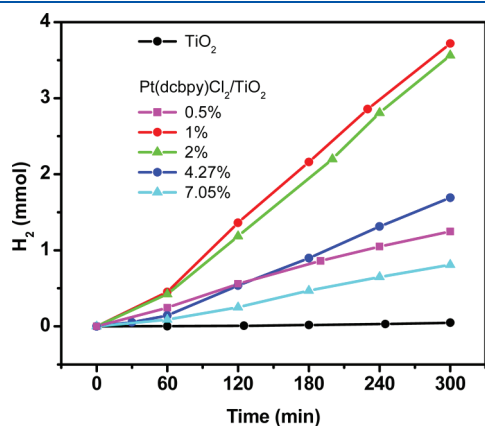
RESULTS AND DISCUSSION

Pt(dcbpy)Cl$_2$ was designed to surface anchor on TiO$_2$ nanoparticles owing to the carboxylic acid groups present on 4,4′-dicarboxylic acid-2,2′-bipyridine (dcbpy) ligand. This yellow complex exhibits a modest extinction coefficient at its absorption peak in the near-visible ($\lambda = 377$ nm, $\varepsilon = 2770$ M^{-1} cm^{-1}), which overlaps the titania band edge. This creates a situation where Pt(dcbpy)Cl$_2$-induced absorbance of bandgap excitation can have a pronounced effect on the resultant material. Minute amounts of aqueous base deprotonates the acids forming carboxylates, promoting the solubility of this complex in water. After stirring mixtures containing Pt(dcbpy)Cl$_2$ in water and TiO$_2$, Pt(dcbpy)Cl$_2$ adsorbed onto TiO$_2$ was readily obtained, whose loading by mass was easily determined by adsorption isotherms derived from UV−vis spectra of the supernatant solutions. When required, 0.1 M KOH was used to desorb surface-anchored Pt^{II} species. (See the Supporting Information for more details.) The various Pt(dcbpy)Cl$_2$/TiO$_2$ materials were tested for hydrogen production upon TiO$_2$ bandgap excitation (3.0 to 3.2 eV) in the presence of hole scavengers, which resulted in the photodeposition (PD) of Pt^0 nanoparticles in all instances. Alcohols such as methanol and ethanol have been widely used as hole scavengers due to the thermodynamic and kinetic favorability of alcohol oxidation by TiO$_2$ valence band holes.[17,43−46] In the current work, we used aqueous media composed of 1:6 MeOH/H$_2$O by volume for all photocatalytic hydrogen-evolving experiments. These experimental conditions ensured efficient hole scavenging during bandgap illumination that positioned the composition to accumulate electrons at titania, termed TiO$_2$(e$^-$) throughout this manuscript. In some instances, Pt^0 nanoparticles were formed via chemical deposition (CD) using direct NaBH$_4$ reduction of select Pt(dcbpy)Cl$_2$/TiO$_2$ compositions, which were compared with the corresponding photodeposited materials.

Atomic resolution STEM images of the 1% Pt(dcbpy)Cl$_2$/TiO$_2$ sample after 5 h of bandgap illumination indicated the presence of Pt nanoparticles (distinguishable as bright areas in Figure 1a), with characteristic lattice fringes indexed to the fcc (111) crystal phase. The high-resolution image in Figure 1a confirms that the lattice spacing is 2.2 Å, whereas the expected value for Pt(111) is $a/\sqrt{3}$ (2.26 Å), where a (3.92 Å) is the lattice constant of bulk Pt.[47] Statistical analysis of multiple STEM images revealed that the formed nanoparticles at 1% loading were ∼1.5 nm in diameter, with a size dispersion of ±0.2 nm. Energy-dispersive X-ray (EDX) spectroscopy measurements confirmed the presence of elemental platinum in these particles (Figure 1b). Most of the remaining signals emanated from the holey carbon substrate and the TiO$_2$ support.

Figure 2 presents the hydrogen evolved versus irradiation time measured as a function of Pt(dcbpy)Cl$_2$ catalyst precursor (mass percent) originally loaded onto the TiO$_2$ surface. These samples contained 25 mg of each Pt(dcbpy)Cl$_2$/TiO$_2$ composition suspended in 25 mL of MeOH/H$_2$O (1:6), ultimately subjected to 300 W broadband Xe lamp illumination. It is important to note that the precursor loading in these samples does not represent the final Pt nanoparticle catalyst loading; the latter is quantified from surface desorption of remnant Pt^{II} molecular species subsequent to 5 h of continuous photocatalysis. The hydrogen evolution yield increases with decreasing surface coverage, exhibiting optimal performance with the 1 to 2% Pt(dcbpy)Cl$_2$/TiO$_2$ composition (Figure 2). The first hour of hydrogen evolution in the in situ photodeposited materials was characterized by a slightly lower rate than the later time periods, behavior attributed to an induction period necessary to form the catalytically active Pt nanoparticles (Figure 2). For this reason, the turnover frequency calculation (TOF = [mol H$_2$ produced] × [mol decomposed Pt^{n+} precursors]$^{-1}$ × s^{-1}) is reported over the time range between 1 and 5 h for these in situ photodeposited materials (Table 1). The 0.5% loading was characterized by a lower hydrogen evolution rate (240 μmol/h) relative to the 1 to 2% loading (800 μmol/h). This observation can be rationalized by the lower surface coverage of the Pt catalyst on TiO$_2$ at loadings below 1%. Related previous optimized systems require the use of ∼0.5 to 1 wt % Pt on TiO$_2$ to achieve optimal catalysis and when translated into the current composition mandates 1 to 2% by mass Pt(dcbpy)Cl$_2$ on TiO$_2$.[20,21,25,43]

An important factor contributing to optimal hydrogen production at 1 to 2% Pt loading and the decrease in catalytic activity

at higher precursor loadings potentially emanates from the absorbance of leftover molecular Pt^{II} species resident on the titania surface. As previously mentioned, Pt(dcbpy)Cl$_2$ is a yellow complex possessing a broad charge transfer absorption band centered at 377 nm with a modest extinction coefficient (ε = 2770 M^{-1} cm^{-1}), which can serve to attenuate photon flux in the vicinity of the bandgap. We postulated that the observed decrease in hydrogen evolution rates as a function of increased surface coverage might simply be reflecting a systematic attenuation in light absorbed by the TiO$_2$. To test this possibility, we used 0.1 M KOH to desorb quantitatively any surface-bound Pt^{II} complexes remaining after 5 h of photocatalytic reaction; specifically, 25 mg of the TiO$_2$/Pt sample (after catalysis) was treated with 25 mL of 0.1 M KOH. The corresponding solutions were centrifuged (10 min, 10 000 rpm) and filtered using a 0.2 μm pore size filter. The photoinitiated hydrogen evolution of the collected solid catalyst was then monitored by GC. This base treatment did not increase the catalytic activity at ≤2% loading. However, the complete removal of the remaining molecular surface-anchored Pt^{II} precursors markedly enhanced the hydrogen evolving activity from 180 to 240 μmol/h of the deposited Pt at 7.05% initial loading (Figure 3a). The same data also imply that the presence of molecular Pt^{II} species on the surface of titania is responsible for a significant amount of light absorption in the vicinity of the bandgap. In fact, the calculated amounts of Pt^{II} precursors remaining on the surface of TiO$_2$ after 5 h of catalysis suggest that only ~10% of the originally present Pt(dcbpy)Cl$_2$ at high surface coverage (7.05% loading) actually decomposed, whereas ~75% of this same molecule decomposed at low surface coverage (1% loading) (Figure 3b). Ultimately at low surface coverage (≤2% by mass of Pt(dcbpy)Cl$_2$), the decomposition was complete after prolonged photolysis (>7 h). The combined results suggest that molecular Pt(dcbpy)Cl$_2$ is more efficiently decomposed to Pt^0 at low surface coverage and exerts a rather substantial UV bandgap absorbance at higher surface coverage.

The data presented in Figure 4 are representative of catalytic hydrogen-evolving samples formed from complete decomposition of the molecular precursors present. In these instances, 1% molecular precursor loading (either Pt(dcbpy)Cl$_2$ or H$_2$PtCl$_6$), followed by broadband irradiation resulted in quantitative Pt^0 deposition, as ascertained by negligible detection of any molecular precursors desorbed from the titania surface. Subsequent to washing, these materials were resuspended in 1:6 MeOH/H$_2$O and tested for their hydrogen photocatalytic activity. Notably, the material isolated after complete PD of Pt(dcbpy)Cl$_2$ (300 μmol/h) significantly outperformed that photodeposited from H$_2$PtCl$_6$ (130 μmol/h) (Figure 4). The hydrogen evolution rate is lower in these particular samples as a result of the catalyst being present in smaller quantities (12 mg as opposed to 25 mg used to obtain the data in Figure 2) and from postphotolysis processing (washing, drying, etc.). The combined data associated with catalytic samples formed from quantitative decomposition of the Pt-based molecular precursors (1% by mass on titania) are collected in Table 2.
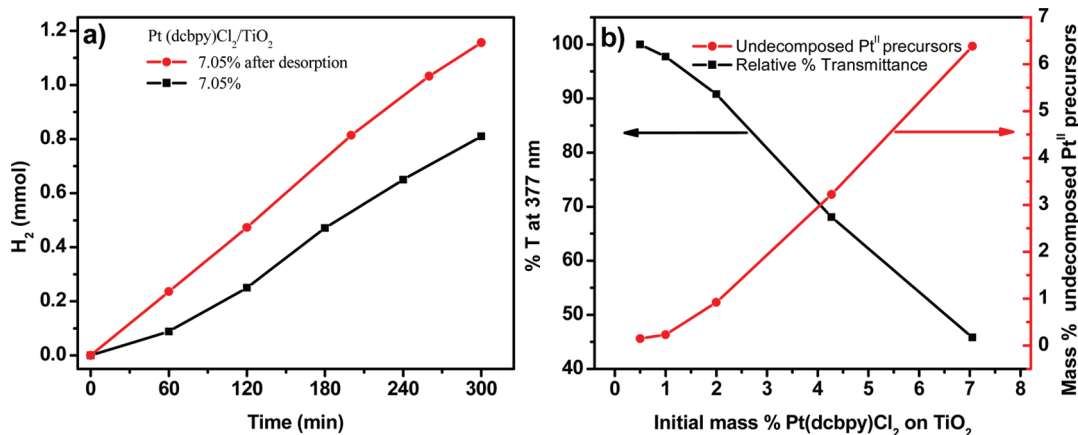
In another set of experiments, chemically deposited platinum nanoparticle performance (produced from NaBH$_4$ reduction) was directly compared with that generated from PD (Figure 5). These measurements were also acquired with 12 mg of each sample suspended in 25 mL of 1:6 MeOH/:H$_2$O. Prior to photocatalysis experiments, each solid was isolated immediately after platinum nanoparticle deposition, after washing and vacuum drying. The sample generated from CD clearly operates at a lower catalytic activity with respect to the one produced via PD (200 and 300 μmol/h, respectively). Because the surface coverage was the same, the TOF follows the same trend (0.24 and 0.36 s^{-1}, respectively) (Figure 5 and Table 2).

Another possible explanation was experimentally tested to rationalize the observation that the 1 to 2% loaded samples
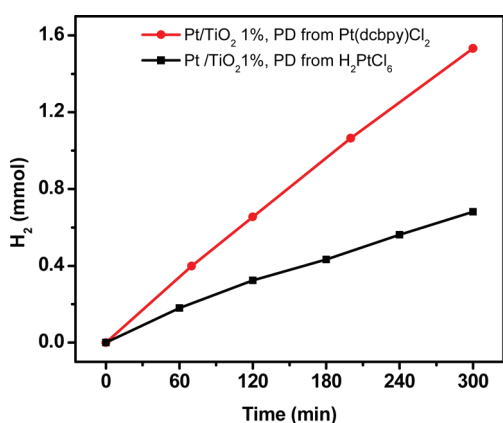

Figure 2. Photochemical hydrogen evolution from 25 mg samples of Pt(dcbpy)Cl$_2$/TiO$_2$ at varied initial surface coverage (specified in legend) suspended in 25 mL of MeOH/H$_2$O (1:6).

Table 1. Summary of Relevant Materials Parameters and In Situ Photocatalytic Activity of 25 mg Pt(dcbpy)Cl$_2$/TiO$_2$ Samples at Different Initial Surface Coverage

surface coverage (%)	activity (μmol·H$_2$/h)^a	precursor decomposed (mg)^b	precursor decomposed (μmol)^b	TOF (s^{-1})^c	Pt(0)$_x$ per mg "N"^{d}	particle size (nm)^e	shell number "n"^{f}	surface Pt "10n^2 + 2"^{f}	Pt atoms "x"^{g}	surface atoms (%)^h	surface TOF (s^{-1})^i
0.5%	250	0.1	0.2	0.35	3.2 × 10^{13}	~1.5	3	92	~150	~60%	0.6
1%	810	0.2	0.4	0.56	6.4 × 10^{13}	~1.5	3	92	~150	~60%	0.9
2%	790	0.28	0.55	0.4	8.8 × 10^{13}	~1.5	3	92	~150	~60%	0.7
4.27%	390	0.28	0.55	0.2	4.3 × 10^{13}	~2	4	162	~310	~50%	0.4
7.05%	180	0.18	0.35	0.14	1.5 × 10^{13}	~2.5	5	252	~560	~45%	0.3

^{a} Photocatalytic activity (μmol H$_2$/h) was measured by GC headspace analysis. ^{b} Amount of decomposed Pt precursor (milligrams and micromole, respectively) was deduced from the quantitative desorption of Pt^{II} precursors. ^{c} Turnover frequencies TOF = [mol H$_2$ produced] × [mol decomposed Pt^{n+} precursors]$^{-1}$ × s^{-1}. ^{d} Number "N" of Pt(0)$_x$ crystallites per milligram of TiO$_2$ was calculated from obtained data. ^{e} Average nanoparticle size (nanometer) was measured by STEM. ^{f} Pt nanoparticle shell number "n" and the magic number of surface atoms "10n^2 + 2" were calculated based on nanoparticle diameter. ^{g} Total number of atoms per nanoparticle was calculated from size distribution data. ^{h} % of surface atoms which was assumed to be catalytically active. ^{i} Surface TOF (s^{-1}) was calculated from TOF and % of surface atoms; see the text for details.

1433

dx.doi.org/10.1021/jp206943s | J. Phys. Chem. C 2012, 116, 1429–1438

Figure 3. (a) Hydrogen evolution increases after removal of the remaining molecular Pt^{II} complexes from the surface of TiO_2 at higher surface coverage, illustrating the absorbance of undecomposed Pt^{II} precursors in the UV region of this sample. (b) Normalized percent transmittance at 377 nm (black line and data points) of five different solutions and the calculated mass of Pt^{II} precursors remaining on the TiO_2 surface (red line and data points), where the unreacted Pt^{II} precursors are systematically desorbed at each percentage loading from the surface of titania after 5 h of photocatalysis.

Figure 4. Photochemical hydrogen evolution from 12 mg of Pt/TiO_2 (1% by mass prepared from complete photodeposition (PD) of $Pt(dcbpy)Cl_2$ on TiO_2, red line and data points) versus the benchmark Pt/TiO_2 (1% by mass prepared by 5 h photodeposition of H_2PtCl_6 on TiO_2, black line and data points) both suspended in 25 mL of MeOH/H_2O (1:6).

outperformed all others in hydrogen production activity (Figure 2); namely, smaller nanoparticles with enhanced catalytic activity[22] were formed at lower surface coverage. Dark-field STEM images of Pt particles at varied surface coverage were quantitatively analyzed. At low loading of $Pt(dcbpy)Cl_2$ (0.5 to 2%), the resulting particles were 1.5 ± 0.2 nm in diameter, whereas at higher coverage (4.27 and 7.05%), they were measurably larger: 1.9 ± 0.3 and 2.5 ± 0.4 nm, respectively. Both the Pt(II) precursor and deposition method influence the Pt particle size. The 1% sample resulting from CD yields Pt(0) nanoparticles that were 2 ± 0.5 nm in diameter, whereas the 1% H_2PtCl_6 photodeposited sample results in the generation of 3 ± 0.6 nm particles (Figure 6). Therefore, a clear variation in the efficiency of hydrogen production with the ultimate size of resultant nanoparticles was observed. In theory, small nanoparticle clusters have more exposed platinum surface area potentially leading to higher catalytic efficiencies.[27] This notion is consistent with the current experimental data and quantified further in Tables 1 and 2. In summary, the higher photocatalytic efficiency of the photodeposited

Pt^0 catalysts from $Pt(dcbpy)Cl_2$ precursors at lower loadings was shown to be correlated to the formation of smaller particles and the absence of possible contaminants when Pt^0 is formed photochemically in situ.

Because of the complexity of heterogeneous photocatalytic materials, the activity in terms of micromoles per hour under defined experimental conditions was used as a metric for the relative performance of different samples throughout the literature as summarized in the cited review article.[9] We also calculated turnover frequencies and surface turnover frequencies for comparative purposes in this study, and these data are summarized in Tables 1 and 2. Assuming spherical $Pt(0)_x$ nanoparticles, one can estimate the average number of Pt atoms (x) present in the nanoparticles in each sample. Full shell nanoparticles are thermodynamically stable and possess lower reactivity for surface growth, so it is expected that transition-metal nanoparticles are centered around "magic number" clusters: $Pt(0)_{13}$, $Pt(0)_{55}$, $Pt(0)_{147}$, $Pt(0)_{309}$, $Pt(0)_{561}$, $Pt(0)_{923}$, and so on.[48] Therefore, using the "magic number" formula for the number of surface atoms ($10n^2 + 2$, where n is the number of shells), we can estimate the percentage of surface atoms (assumed to be catalytically active) in each sample and subsequently calculate a surface turnover frequency, surface TOF (s^{-1}) = [TOF (s^{-1})] × (fraction of surface atoms)$^{-1}$, whose values are collected in Table 1.[27,48−50] All surface TOF values reported were calculated subsequent to the observed induction period for nanoparticle formation present for the in situ photodeposited samples (Figure 2 and Table 1). In addition, the number (N) of $Pt(0)_x$ nanoparticles per mass of TiO_2 (milligram) were calculated (Tables 1 and 2) using eq 1

$$NPt(0)_x = n \times N_a \times x^{-1} \times (\text{mass of } TiO_2)^{-1} \qquad (1)$$

Here n is the number of moles of decomposed Pt precursor, N_a is Avogadro's number, and x is the number of Pt atoms per $Pt(0)_x$ cluster.
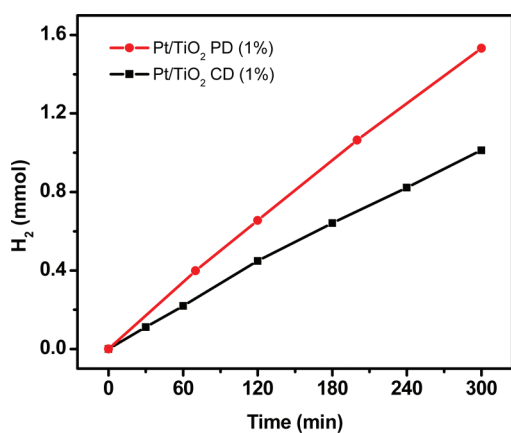
The trends found for the photocatalytic activities in terms of both TOF and surface TOF clearly reflect changes in catalytic behavior in different samples resulting from two main factors discussed throughout this report. The first relates to the absorbance in the UV due to undecomposed Pt^{II} precursors at high surface coverage ultimately resulting in diminished catalytic

Table 2. Summary of Relevant Materials Parameters and Photocatalytic Activity of 12 mg Pt⁰/TiO₂ Composites Formed from Different Molecular Precursors (1% Pt(dcbpy)Cl₂ or H₂PtCl₆) Subsequent to Recovery Following Photodeposition (PD) or Chemical Deposition (CD)

Pt⁰ deposition method	activity (μmol·H₂/h)[a]	precursor decomposed (mg)[b]	precursor decomposed (μmol)[b]	TOF (s⁻¹)[c]	Pt(0)ₓ per mg "N"[d]	particle size (nm)[e]	shell number "n"[f]	surface Pt "$10n^2 + 2$"[f]	Pt atoms "x"[g]	surface atoms (%)[h]	surface TOF (s⁻¹)[i]
PD from Pt(dcbpy)Cl₂	300	0.12	0.23	0.36	7.7×10^{13}	~1.5	3	92	~150	~60%	0.6
CD from Pt(dcbpy)Cl₂	200	0.12	0.23	0.24	3.7×10^{13}	~2	4	162	~310	~50%	0.5
PD from H₂PtCl₆	130	0.12	0.23	0.16	1.3×10^{13}	~3	6	362	~920	~40%	0.4

[a] Photocatalytic activity (μmol H₂/h) was measured by GC headspace analysis. [b] Amount of decomposed Pt precursor (milligram and micromole, respectively) based on complete decomposition of Pt^{n+} precursors. [c] Turnover frequencies TOF = [mol H₂ produced] × [mol decomposed Pt^{n+} precursors]⁻¹ × s⁻¹. [d] Number "N" of Pt(0)ₓ crystallites per milligram of TiO₂ was calculated from obtained data. [e] Average nanoparticle size (nanometer) was measured by STEM. [f] Pt nanoparticle shell number n and the magic number of surface atoms $10n^2 + 2$ were calculated based on nanoparticle diameter. [g] Total number of atoms per nanoparticle was calculated from size distribution data. [h] % of surface atoms which was assumed to be catalytically active. [i] Surface TOF (s⁻¹) was calculated from TOF and % of surface atoms; see the text for details.


Figure 5. Comparison of hydrogen evolution from 12 mg of Pt(dcbpy)Cl₂/TiO₂ using photodeposition (PD) (red line and data points) and chemical deposition (CD) (black line and data points), respectively. Both samples were isolated after complete decomposition of Pt(dcbpy)Cl₂ on the titania surface.

activity. To elucidate further this concept, surface TOF values can be useful because these values are corrected for the fraction of exposed Pt atoms. For comparative purposes, refer to the surface TOF of the in situ photodeposited samples at different surface coverage (Table 1). The surface TOF is clearly higher at low catalytic loadings ($\leq$2%). Second, the larger number of surface atoms produced in smaller nanoparticles exhibit higher catalytic activity and improved TOFs, consistent with the materials produced from photodecomposition of Pt(dcbpy)Cl₂ resident on titania at 1 to 2% by mass. The inadequate surface coverage of Pt on TiO₂ at 0.5% loading is deemed responsible for the lower catalytic activity (240 μmol/h) because the TOF, which corrects for the amount of Pt decomposed on TiO₂ is 0.35 s⁻¹, greater than the TOF obtained in the 4.27 and 7.05% samples, 0.2 s⁻¹ and 0.14 s⁻¹, respectively. This trend would be anticipated given that the samples at higher loading suffer from Pt^{II} precursor-induced competitive absorbance of bandgap photons and the subsequent formation of larger Pt⁰ nanoparticles.

In two distinct experiments operated under different conditions, liquid Hg and gaseous CO (at 1 atm) were introduced into the photoreaction mixture, and the hydrogen evolution was

significantly attenuated (Figure 7). Hydrogen evolution catalysis at Pt⁰ is known to be poisoned by mercury because of the formation of a Hg/Pt amalgamate.[31] In the present compositions, the Hg strongly interacted with these samples to the point that most of the suspended material accumulated and bound to the mercury at the bottom of the photoreactor. Platinum is also known to have high surface adsorption capacity for CO, which easily passivates the surface upon binding.[30] At 1 atm pressure (gas bubbled through the aqueous suspension), the CO substantially inactivates the photocatalytic evolution of H₂ gas from the samples. The two combined heterogeneous poisoning tests strongly suggest that the catalysis responsible for H₂ generation is indeed heterogeneous in nature and results from the Pt nanoscopic particles embedded on the titania surface rather than from any remnant molecular Pt^{II} species. Similar data were obtained after aqueous base was utilized to remove all molecular Pt^{II} complexes from the titania surface after several hours of photoreaction.

DFT and TD-DFT calculations have suggested that Pt(dcbpy)Cl₂ is stable upon one electron reduction. However, photoexcitation of this reduced compound with visible light is expected to result in Pt⁰ agglomerates when these molecules are in solution.[51] Such a mechanism is qualitatively consistent with the PD of Pt nanoparticles seen in all of the materials presented herein.[51] Whereas this mechanism justifies the photodecomposition of Pt^{II} molecular complexes under light illumination, Pt nanoparticle formation has also been observed from Pt^{n+} salt precursors, starting with the reduction of Pt^{n+} into Pt⁰ by the conduction band electrons of TiO₂ upon bandgap excitation, where Pt⁰ adsorbed on the titania surface ultimately agglomerates into small crystallites.[25] Under equilibrium conditions, the flatband potential of TiO₂ at the TiO₂/electrolyte interface is defined by $V_{fb} = -0.2 - 0.059$ pH $= -0.613$ V at pH 7.[52,53] In a qualitative experiment, electrons on titania (TiO₂(e⁻)s) were produced electrochemically in an argon-saturated H-cell by biasing a TiO₂ film on a FTO electrode at -1000 mV versus Ag/AgCl in 0.1 M sodium phosphate buffer at pH 7, in conjunction with a Pt wire counter electrode in a standard three-electrode arrangement. At this potential, which roughly supplies 390 mV overpotential for hydrogen evolution at pH 7.0, electrons become trapped rapidly in the conduction band of TiO₂, and because TiO₂ is not a good electrocatalyst for hydrogen evolution itself, the resultant film turns from white to blue, indicating the presence of TiO₂(e⁻)

1435

dx.doi.org/10.1021/jp206943s |J. Phys. Chem. C 2012, 116, 1429–1438
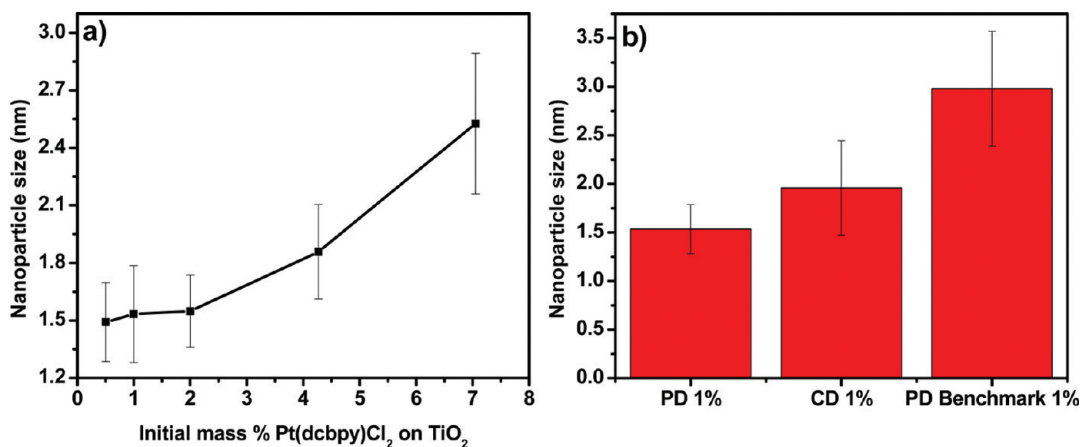
Figure 6. (a) Variation of particle size as a function of Pt(dcbpy)Cl$_2$ initial surface coverage on TiO$_2$. (b) Comparison of particle size from 1% Pt(dcbpy)Cl$_2$ photodeposited (PD), chemically deposited (CD), and the 1% H$_2$PtCl$_6$ PD benchmark.
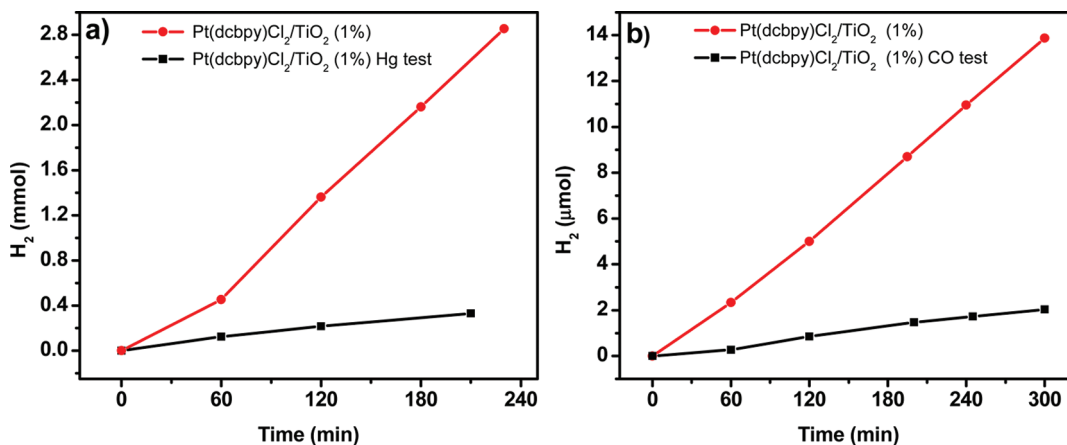
Figure 7. (a) Mercury poisoning test performed on samples produced via photolysis of 1% Pt(dcbpy)Cl$_2$ by mass adsorbed on titania with Pt(0) formed in situ. (b) CO (1 atm) inhibition experiment performed on photodeposited catalytic samples subsequent to Pt(0) photodeposition. Hydrogen evolution decreases dramatically in the presence of Hg and CO in 1% Pt(dcbpy)Cl$_2$/TiO$_2$ suggesting that the catalyst is indeed heterogeneous and has its origin in the formed Pt nanoparticles.
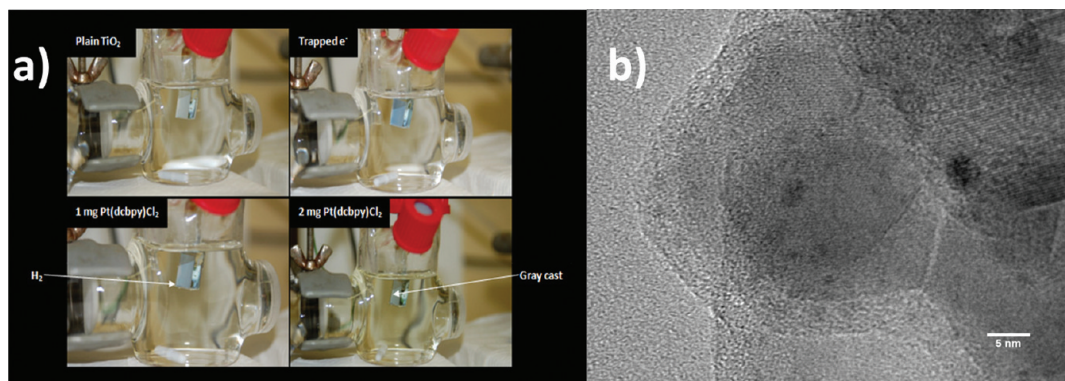
Figure 8. (a) Qualitative electron trapping experiment showing the color change of the white TiO$_2$ film into blue due to trapped electrons resulting from −1000 mV versus Ag/AgCl applied bias in 0.1 M sodium phosphate buffer at pH 7.0. Ultimately, this material turns gray after the addition of Pt(dcbpy)Cl$_2$ to the solution and removal of the bias. (b) TEM image of the scraped film after the experiment indicates the presence of Pt nanoparticles (black) on the TiO$_2$ support (lighter), 5 nm scale bar.

(Figure 8).[54] The electrochemical bias was removed after 5 min, then Pt(dcbpy)Cl$_2$ in slightly basic water was injected in the working side of the electrochemical cell under an argon atmosphere in the dark, turning the TiO$_2$ film into a gray cast signaling

the formation of metallic platinum. Hydrogen could be readily detected from the headspace by GC after the injection of this molecular precursor and the subsequent formation of platinum nanoparticles, ultimately confirmed using TEM. This experiment verifies that $TiO_2(e^-)$s are likely responsible for the reduction of the surface-anchored Pt^{II} complex into Pt^0, which ultimately leads to heterogeneous hydrogen production as a dark reaction. However, this does not necessarily imply that the one-electron reduced $Pt(dcbpy)Cl_2$ complex is unstable, as multiple electrons can be simultaneously delivered to the molecules under these experimental conditions.

Meyer and coworkers have reported a similar observation on $Ru(dcbq)(bpy)_2/TiO_2$ and $hemin/TiO_2$ systems where $TiO_2(e^-)$ afforded the reduction of these surface-anchored compounds.[55] In a separate experiment, $Pt(dcbpy)Cl_2/TiO_2$ (1%) in pure water was irradiated using broadband white light illumination from a Xe lamp, and the solid isolated after irradiation possessed a gray cast suggesting the formation of Pt nanoparticles. This experiment confirmed that $TiO_2(e^-)$ derived from a photochemical experiment can reduce $Pt(dcbpy)Cl_2$ into Pt^0 nanoparticles in the absence of hole scavengers. Similar results have been described in the photochemical Pt deposition on TiO_2 from various Pt complexes in aqueous media.[25,52] It is important to note that in the current photocatalytic H_2 production experiments over titania, CO_2 was also qualitatively detected in the reactor headspace by GC, verifying the oxidation of MeOH by hole migration to the surface of TiO_2. For more details of methanol decomposition products generated (HCHO, CO_2, etc.) and the associated plausible mechanisms, please refer to the literature.[43]

CONCLUSIONS

Bandgap excitation of TiO_2 containing surface-anchored Pt-$(dcbpy)Cl_2$ molecules in 1:6 methanol/water results in the formation of Pt^0 nanoparticles that subsequently photocatalyze the reduction of protons into hydrogen. Some of the lowest $Pt(dcbpy)Cl_2$ surface coverage (1 to 2% loading by mass) produced materials exhibiting the highest photocatalytic performance, which significantly outperformed all other surface coverage and the benchmarks. The CD of this catalyst via $NaBH_4$ reduction on TiO_2 gave rise to slightly inferior catalytic materials, suggesting that in situ PD of surface-anchored precursors represents a superior method for growing hydrogen-evolving Pt^0 clusters. At low surface coverage, smaller nanoparticles prevail affording higher surface areas for catalysis. A rather substantial absorbance emanating from unreacted Pt^{II} precursors was observed, which dramatically decreased hydrogen evolution at higher surface coverage. The complete decomposition of the precursor was only achieved only at low percentage loading (<2% by mass of $Pt(dcbpy)Cl_2$ on TiO_2) upon extended photolysis. The combined data suggest that 1 to 2% $Pt(dcbpy)Cl_2$ on TiO_2 represents the minimum surface coverage necessary to produce highly efficient catalytic activity owing to the small nanoparticle diameters generated (1.5 nm), possibly stabilized by both dcbpy and chloride ligands, and the reduced interfering UV absorbance associated with unreacted Pt^{II} precursor molecules. This study promotes the economic usage of noble metals in the area of hydrogen production catalysis, as demonstrated by using modest amounts of the surface-anchored molecular precursor Pt-$(dcbpy)Cl_2$ for the generation of high activity and monodisperse Pt^0 nanoparticles on titania surfaces.

ASSOCIATED CONTENT

⑤ Supporting Information. Histograms for Pt size distributions, STEM images, photographs of materials, additional spectroscopic data, and experimental details. This material is available free of charge via the Internet at http://pubs.acs.org.

AUTHOR INFORMATION

Corresponding Author
*E-mail: castell@bgsu.edu.

ACKNOWLEDGMENT

REFERENCES

(1) Gray, H. B.; Maverick, A. W. *Science* **1981**, *214*, 1201–1205.
(2) Heyduk, A. F.; Nocera, D. G. *Science* **2001**, *293*, 1639–1641.
(3) *Energy Resources through Photochemistry and Catalysis*; Gratzel, M., Ed.; Academic Press: New York, 1983.
(4) *Photochemical Energy Conversion*; Norris, J. R., Jr., Meisel, D., Eds.; Elsevier: New York, 1989.
(5) Esswein, A. J.; Nocera, D. G. *Chem. Rev.* **2007**, *107*, 4022–47.
(6) *Homogeneous Photocatalysis*; Chanon, M., Ed.; John Wiley & Sons: Chichester, U.K., 1997.
(7) *Photoinduced Electron Transfer*; Fox, M. A., Chanon, M., Eds.; Elsevier: Amsterdam, 1988.
(8) *Photogeneration of Hydrogen*; Harriman, A., West, M. A., Eds.; Academic Press: London, 1982.
(9) Kudo, A.; Miseki, Y. *Chem. Soc. Rev.* **2009**, *38*, 253–278.
(10) Rau, S.; Schafer, B.; Gleich, D.; Anders, E.; Rudolph, M.; Friedrich, M.; Gorls, H.; Henry, W.; Vos, J. G. *Angew. Chem., Int. Ed.* **2006**, *45*, 6215–6218.
(11) Ozawa, H.; Yokoyama, Y.; Haga, M.; Sakai, K. *Dalton Trans.* **2007**, 1197–1206.
(12) Sakai, K.; Ozawa, H. *Coord. Chem. Rev.* **2007**, *251*, 2753–2766.
(13) Du, P.; Schneider, J.; Jarosz, P.; Zhang, J.; Brennessel, W. W.; Eisenberg, R. *J. Phys. Chem. B* **2007**, *111*, 6887–6894.
(14) Jarosz, P.; Du, P.; Schneider, J.; Lee, S.-H.; McCamant, D.; Eisenberg, R. *Inorg. Chem.* **2009**, *48*, 9653–9663.
(15) Zhang, J.; Du, P.; Schneider, J.; Jarosz, P.; Eisenberg, R. *J. Am. Chem. Soc.* **2007**, *129*, 7726–7727.
(16) Lei, P.; Hedlund, M.; Lomoth, R.; Rensmo, H.; Johansson, O.; Hammarstroem, L. *J. Am. Chem. Soc.* **2008**, *130*, 26–27.
(17) Meyer, S.; Saborowski, S.; Schaefer, B. *ChemPhysChem* **2006**, *7*, 572–574.
(18) Finney, E. E.; Finke, R. G. *Inorg. Chim. Acta* **2006**, *359*, 2879–2887.
(19) Widegren, J. A.; Finke, R. G. *J. Mol. Catal. A: Chem.* **2003**, *198*, 317–341.
(20) Du, P.; Schneider, J.; Li, F.; Zhao, W.; Patel, U.; Castellano, F. N.; Eisenberg, R. *J. Am. Chem. Soc.* **2008**, *130*, 5056–5058.
(21) Zhao, W.; Sun, Y.; Castellano, F. N. *J. Am. Chem. Soc.* **2008**, *130*, 12566–12567.
(22) Yamamoto, K.; Imaoka, T.; Chun, W.-J.; Enoki, O.; Katoh, H.; Takenaga, M.; Sonoi, A. *Nat. Chem.* **2009**, *1*, 397–402.
(23) Courbon, H.; Herrmann, J. M.; Pichat, P. *J. Phys. Chem.* **1984**, *88*, 5210–5214.

(24) Disdier, J.; Herrmann, J. M.; Pichat, P. *J. Chem. Soc., Faraday Trans. 1* **1983**, *79*, 651–660.

(25) Herrmann, J. M.; Disdier, J.; Pichat, P. *J. Phys. Chem.* **1986**, *90*, 6028–6034.

(26) Kohler, J. U.; Bradley, J. S. *Catal. Lett.* **1997**, *45*, 203–208.

(27) Aiken, J. D.; Finke, R. G. *J. Mol. Catal. A: Chem.* **1999**, *145*, 1–44.

(28) Mondloch, J. E.; Yan, X. H.; Finke, R. G. *J. Am. Chem. Soc.* **2009**, *131*, 6389–6396.

(29) Ott, L. S.; Finke, R. G. *Coord. Chem. Rev.* **2007**, *251*, 1075–1100.

(30) Sharma, S.; Ganguly, A.; Papakonstantinou, P.; Miao, X.; Li, M.; Hutchison, J. L.; Delichatsios, M.; Ukleja, S. *J. Phys. Chem. C* **2010**, *114*, 19459–19466.

(31) Anton, D. R.; Crabtree, R. H. *Organometallics* **1983**, *2*, 855–859.

(32) Wang, C.; Yin, L.; Zhang, L.; Liu, N.; Lun, N.; Qi, Y. *ACS Appl. Mater. Interfaces* **2010**, *2*, 3373–3377.

(33) Ohtani, B.; Iwai, K.; Nishimoto, S.-i.; Sato, S. *J. Phys. Chem. B* **1997**, *101*, 3349–3359.

(34) Price, J. H.; Williamson, A. N.; Schramm, R. F.; Wayland, B. B. *Inorg. Chem.* **1972**, *11*, 1280–1284.

(35) Ozawa, H.; Haga, M.; Sakai, K. *J. Am. Chem. Soc.* **2006**, *128*, 4926–4927.

(36) Garelli, N.; Vierling, P. *J. Org. Chem.* **1992**, *57*, 3046–3051.

(37) Wimmer, S.; Castan, P.; Wimmer, F. L.; Johnson, N. P. *J. Chem. Soc., Dalton Trans.* **1989**, 403–412.

(38) Barnett, R. *Biochimie* **1978**, *60*, 859–867.

(39) Baran, V. *Coord. Chem. Rev.* **1971**, *6*, 65–93.

(40) Erickson, L. E.; Erickson, H. L.; Meyer, T. Y. *Inorg. Chem.* **1987**, *26*, 997–999.

(41) Gill, D. S.; Rosenberg, B. *J. Am. Chem. Soc.* **1982**, *104*, 4598–4604.

(42) Zhao, W.; Chen, C.; Li, X.; Zhao, J.; Hidaka, H.; Serpone, N. *J. Phys. Chem. B* **2002**, *106*, 5022–5028.

(43) Highfield, J. G.; Chen, M. H.; Nguyen, P. T.; Chen, Z. *Energy Environ. Sci.* **2009**, *2*, 991–1002.

(44) Kawai, T.; Sakata, T. *J. Chem. Soc., Chem. Commun.* **1980**, 694–695.

(45) Sakata, T.; Kawai, T. *Chem. Phys. Lett.* **1981**, *80*, 341–344.

(46) Pichat, P.; Herrmann, J. M.; Disdier, J.; Courbon, H.; Mozzanega, M. N. *New J. Chem.* **1981**, *5*, 627–636.

(47) Kamperman, M.; Burns, A.; Weissgraeber, R.; van Vegten, N.; Warren, S. C.; Gruner, S. M.; Baiker, A.; Wiesner, U. *Nano Lett.* **2009**, *9*, 2756–2762.

(48) Watzky, M. A.; Finke, R. G. *Chem. Mater.* **1997**, *9*, 3083–3095.

(49) Schmid, G. *Endeavour* **1990**, *14*, 172–178.

(50) Schmid, G. *Chem. Rev.* **1992**, *92*, 1709–1727.

(51) Roy, L. E.; Scalmani, G.; Kobayashi, R.; Batista, E. R. *Dalton Trans.* **2009**, 6719–6721.

(52) Borgarello, E.; Serpone, N.; Emo, G.; Harris, R.; Pelizzetti, E.; Minero, C. *Inorg. Chem.* **1986**, *25*, 4499–4503.

(53) Ward, M. D.; White, J. R.; Bard, A. J. *J. Am. Chem. Soc.* **1983**, *105*, 27–31.

(54) Boschloo, G.; Fitzmaurice, D. *J. Phys. Chem. B* **1999**, *103*, 7860–7868.

(55) Staniszewski, A.; Morris, A. J.; Ito, T.; Meyer, G. J. *J. Phys. Chem. B* **2007**, *111*, 6822–6828.